Space Weather

RESEARCH ARTICLE
10.1029/2024SW004010

Thermospheric Neutral Density Data Assimilation System Based on the Whole Atmosphere Model During the November 2003 Storm

Ching-Chung Cheng[1], Timothy Fuller-Rowell[1,2,3], Eric K. Sutton[3], Tzu-Wei Fang[2], Jann-Yenq Liu[4], and Daniel R. Weimer[5]

[1]Cooperative Institute for Research in Environmental Sciences, University of Colorado Boulder, Boulder, CO, USA, [2]Space Weather Prediction Center, NOAA, Boulder, CO, USA, [3]SWx TREC, University of Colorado Boulder, Boulder, CO, USA, [4]Department of Space Science and Engineering, National Central University, Taoyuan City, Taiwan, [5]Center for Space Science and Engineering Research, Virginia Tech, Blacksburg, VA, USA

Key Points:

- Iterative Driver Estimation and Assimilation (IDEA) data assimilation system greatly improves the Whole Atmosphere Model (WAM) thermospheric neutral density nowcasting capability
- Different locations of observed and modeled high-latitude density hole structures lead to discrepancy between Challenging Mini-Satellite Payload and the model output
- IDEA output is validated against Global Ultraviolet Imager data, indicating a potential use case for limb-scan measurements in the WAM neutral density forecast

Correspondence to:
C.-C. Cheng,
Ching-Chung.Cheng@colorado.edu

Citation:
Cheng, C.-C., Fuller-Rowell, T., Sutton, E. K., Fang, T.-W., Liu, J.-Y., & Weimer, D. R. (2024). Thermospheric neutral density data assimilation system based on the Whole Atmosphere Model during the November 2003 storm. *Space Weather*, *22*, e2024SW004010. https://doi.org/10.1029/2024SW004010

Received 23 MAY 2024
Accepted 13 SEP 2024

Author Contributions:
Conceptualization: Ching-Chung Cheng, Timothy Fuller-Rowell, Tzu-Wei Fang
Data curation: Ching-Chung Cheng, Eric K. Sutton
Formal analysis: Ching-Chung Cheng, Timothy Fuller-Rowell
Funding acquisition: Timothy Fuller-Rowell, Eric K. Sutton, Tzu-Wei Fang
Investigation: Ching-Chung Cheng, Timothy Fuller-Rowell, Eric K. Sutton
Methodology: Ching-Chung Cheng, Timothy Fuller-Rowell, Eric K. Sutton, Tzu-Wei Fang
Project administration: Timothy Fuller-Rowell, Eric K. Sutton, Tzu-Wei Fang
Resources: Eric K. Sutton, Daniel R. Weimer

Abstract The Iterative Driver Estimation and Assimilation (IDEA) data assimilation technique was used with the Whole Atmosphere Model (WAM) to improve neutral density specification in the upper thermosphere. Two different neutral density data sources were examined to enhance the capability of simulating the global thermospheric state. The first were accelerometer estimates of neutral density from the Challenging Mini-Satellite Payload (CHAMP) satellite. The second were neutral density estimates from the Global Ultraviolet Imager (GUVI) limb-scan airglow observations aboard the Thermosphere Ionosphere Mesosphere Energetics and Dynamics satellite. Due to the intensity of the November 2003 storm, two changes were necessary in WAM. The first was allowing the Kp geomagnetic index to exceed 9 and the second was changing the relationship between Kp and the solar wind parameters used to drive the model. With these changes, results show that IDEA effectively captures the thermospheric neutral density at the CHAMP satellite altitude and follows the time-dependence through the November 2003 storm period. Furthermore, a cross-comparison was conducted with the GUVI dayside limb scan measurements. GUVI neutral densities within 270–320 km show the closest agreement with WAM when CHAMP data was assimilated by IDEA. We speculate on the potential for observations from GUVI at 300 km to be used as a data source in the IDEA-WAM simulations. These simulations demonstrate the utility of the IDEA data assimilation technique with physical models and that using either accelerometer observations or ultraviolet airglow limb measurement during extreme storm periods could be used.

Plain Language Summary Strong variations in the neutral density of the thermosphere heavily impact the position of low Earth orbit objects as they respond to radiative inputs from the Sun in the extreme ultraviolet (UV) wavelength range, energetic particle precipitation in the auroral regions, and global-scale electrical currents generated during geomagnetic storms. In this study, the Iterative Driver Estimation and Assimilation (IDEA) data assimilation technique was used with the Whole Atmosphere Model (WAM) to improve neutral density specification in the upper thermosphere. The Challenging Mini-Satellite Payload (CHAMP) satellite and the Global Ultraviolet Imager (GUVI) limb scan UV airglow observations aboard the Thermosphere Ionosphere Mesosphere Energetics and Dynamics (TIMED) satellite were examined to enhance the capability of simulating the global thermospheric state. Results show that IDEA effectively captures the thermospheric neutral density at the CHAMP satellite altitude throughout the November 2003 storm period. Furthermore, GUVI limb scan measurements on the dayside were cross-compared with IDEA densities. We speculate on the potential for observations from GUVI during the daytime to be used as a data source in the IDEA-WAM simulations. This study demonstrates data assimilative physical models are capable of improving neutral density specification for better orbit determination and prediction of low Earth orbiting satellites.

1. Introduction

In recent decades, the accurate specification and forecasting of the thermospheric state has grown increasingly important within the space physics and satellite owner/operator communities. Variations in neutral density lead to dynamic drag forces on low Earth orbit (LEO) satellites flying through the thermosphere, which in turn causes orbital track changes (Berger et al., 2020). Given that the physics-based general circulation models (GCMs) are generally considered the most powerful tool in understanding the complicated three-dimensional time-dependent

Software: Ching-Chung Cheng, Eric K. Sutton
Supervision: Timothy Fuller-Rowell, Jann-Yenq Liu
Validation: Ching-Chung Cheng
Writing – original draft: Ching-Chung Cheng
Writing – review & editing: Ching-Chung Cheng, Timothy Fuller-Rowell, Eric K. Sutton, Tzu-Wei Fang

behavior of Earth's atmosphere, numerous efforts have been made to improve the thermospheric quantities such as neutral temperature, density, composition, and winds through the assimilation of observations into physics-based GCMs (e.g., Cantrall et al., 2019; Cierpik et al., 2003; Codrescu et al., 2004, 2022; Lomidze & Scherliess, 2015; Matsuo et al., 2013; Mehta et al., 2019; Mlynczak et al., 2018; Ruan et al., 2018; Sutton, 2018; Weimer et al., 2020). Matsuo et al. (2013) presented an application of ensemble Kalman filtering (EnKF) to a GCM of the thermosphere and ionosphere by ingesting the electron density of COSMIC/FORMOSAT-3 and the neutral mass density of the Challenging Mini-Satellite Payload (CHAMP) satellite, and showed that assimilation of the electron density profiles and the in situ neutral mass density observations into the Thermosphere-Ionosphere-Electrodynamics General Circulation Model (TIEGCM) is capable of improving the neutral density specification. They also showed that the $F_{10.7}$ index can be inferred from the neutral mass density by using the EnKF, and that it impacts the global neutral density specification.

Sutton (2018) developed a novel physics-based data assimilation technique, Iterative Reinitialization, Driver Estimation, and Assimilation (referred to as IDEA hereafter), to minimize the root-mean-square errors (RMSe) of log density between a model and observed data by iteratively estimating solar and geophysical drivers. IDEA iteratively estimates these external drivers and reinitializes the model for a period extending far enough into the past to let the model respond accordingly. After convergence is attained, the data assimilation window moves ahead 3 hr into the future. By ingesting neutral mass density measurements from low-Earth orbiting accelerometers, Sutton (2018) showed that the IDEA technique greatly reduces RMSe of the physics-based model relative to ingested observations from the CHAMP satellite as well as to an independent validation data set from the Gravity Recovery And Climate Experiment satellite during a long-term simulation in 2003, a period consisting of a wide range of solar and geomagnetic activity levels. They demonstrated that IDEA, an accurate and robust physics-based method, is capable of specifying neutral density during both quiet and disturbed times. However, Sutton (2018) pointed out that Kp estimates are likely to be correlated with those of $F_{10.7}$, making it difficult to separate the two effects during the estimation procedure. Additionally, the 3-hr advancement of the data assimilation window used in Sutton (2018), while established in order to maintain observability of estimated parameters based on the information available from the assimilation data, may not be sufficient to capture some of the rapid changes in the thermosphere during extreme storm periods.

The geomagnetic storm on 20 November 2003 is widely recognized as one of the largest geomagnetic storms during the 23rd solar cycle, as measured by the Dst index (−422 nT). Numerous measurements acquired during the storm period have been analyzed over the past decades (e.g., Bortnik et al., 2006; Bruinsma et al., 2006; Foster et al., 2005; Liu & Lühr, 2005; Meier et al., 2005). Several model simulations have also been conducted to understand how this superstorm affected the terrestrial magnetic fields and subsequently influenced the atmosphere (Fok et al., 2011; Gardner et al., 2018; Weimer et al., 2023). Meier et al. (2005) used the Global Ultraviolet Imager (GUVI) aboard the Thermosphere Ionosphere Mesosphere Energetics and Dynamics satellite (TIMED) neutral compositions/temperature, and compared them with the TIEGCM simulation. They found that the model simulations of the thermospheric response exhibited good agreement with GUVI data prior to the peak of the storm on 20 November, but notable discrepancies between data and model were seen during the main and recovery phases of the storm.

In 2021, a physical model of the Whole Atmosphere Model (WAM) coupled to an Ionosphere Plasmasphere Electrodynamic plasma component was transitioned into operations by NOAA's Space Weather Prediction Center. In this study, in order to enhance the nowcasting capabilities of WAM, neutral density observations from CHAMP satellite accelerometer are assimilated into WAM using the IDEA scheme in the upper thermosphere. In addition, the WAM densities are cross-compared with neutral densities from GUVI dayside limb scan UV airglow measurements in order to validate the model output while exploring potential neutral density data sources for future applications of neutral density data assimilation in WAM.

2. Model and Data

WAM is an extension of the Global Forecast System (GFS, Han & Pan, 2011; Juang, 2011, 2014; NCEP, 2015; Yang et al., 2006, 2008) with a spectral hydrostatic dynamical core. WAM includes additional species, allows for variable specific heat and gas constant, and utilizes an enthalpy thermodynamic variable. The model is extended to 150 vertical levels, with a vertical resolution of a quarter pressure scale height, on a hybrid pressure-sigma grid, spanning Earth's atmosphere from the surface to approximately 3×10^{-7} Pa (400–600 km depending on levels of

solar activity) (see https://www.swpc.noaa.gov/products/wam-ipe). WAM includes all GFS lower atmospheric physics processes via the common column-physics interface. These include radiative processes, hydrological cycle, planetary boundary-layer and surface exchange processes, parameterized ozone photochemistry, orographic gravity waves, and others (Akmaev et al., 2008). WAM ionosphere-thermosphere (I-T) physics extends the GFS model physical processes, which includes UV and EUV radiative heating, parameterized NO, O_3, CO_2, and H_2O infrared radiative cooling with the breakdown of local thermodynamic equilibrium, non-orographic gravity waves, viscosity, Joule and auroral heating, ion drag, and molecular diffusion of heat, momentum, and species (Akmaev, 2001; Fuller-Rowell & Rees, 1980; Fuller-Rowell et al., 1996). The high-latitude electric potential model is based on Weimer (2005). In this study, WAM is run with a triangularly truncated spherical harmonic expansion of degree and order 62 (T62) equivalent to a horizontal resolution of ~180 km in latitude-longitude. In operations, WAM is driven by the average of the daily $F_{10.7}$ solar radio flux at 10.7 cm wavelength (measured in solar flux unit—sfu, where 1 sfu = 10^{-22} W m^{-2} Hz^{-1}) and the average of the previous 41-day daily $F_{10.7}$, centered on the day of interest, an average of the previous 24 hr of Kp, hemispheric auroral power (Hp), interplanetary magnetic field (IMF) B_z and B_y components, solar wind velocity (V_{sw}), and solar wind plasma density as the input drivers. In the free-run mode, WAM can be operated with observed solar wind drivers or, alternatively, the solar wind drivers can be derived from Kp based on empirical formulas. These drivers were linearly interpolated to the 1-min temporal resolution of WAM prior to being ingested into the model.

The IDEA assimilative system was developed by Sutton (2018). IDEA targets aspects of the I-T model exhibiting the most uncertainty while preserving, wherever possible, the internal self-consistency of the I-T model. IDEA modifies the solar flux (i.e., $F_{10.7}$) and geomagnetic (i.e., Kp) drivers by ingesting the observed I-T data, and iteratively reinitializes the model for 24 hr into the past to bring the model into agreement with neutral density data from observations. Note that the $F_{10.7}$ used in this process is the solar activity factor given by $F_{10.7} = (F_{10.7d} + F_{10.7A})/2$, where $F_{10.7d}$ is the daily solar radio flux of 10.7 cm wavelength and $F_{10.7A}$ is the 81-day average of the daily $F_{10.7}$ centered on the day of interest (Hinteregger et al., 1981; Richards et al., 1994). In Sutton (2018), a 1-day effective $F_{10.7}$ and three latest effective 3-hr Kp indices are estimated repeatedly until the convergence is achieved, and the $F_{10.7}$ and Kp are updated with the newly estimated ones. In this work, we test whether, the quickly varying conditions that occur during strongly disturbed geomagnetic conditions can be captured in shorter than 3-hr increments. In addition, we attempt to limit the correlation between Kp and $F_{10.7}$ correction. These efforts will be elaborated on in Section 4.

The CHAMP satellite was launched on 15 July 2000 into a near-circular orbit with an inclination of 87.25°, and orbital period of 93 min. During the 20 November 2003 geomagnetic storm, the satellite altitude varied between 380 and 420 km. The satellite carried a very sensitive accelerometer, and the acceleration due to air drag has been used to derive the neutral density (Bruinsma et al., 2004; Doornbos et al., 2010; Liu et al., 2005; Mehta et al., 2017; Siemes et al., 2023; Sutton, 2009; Sutton et al., 2005, 2007). The derived neutral density data are further binned and averaged along the satellite's orbit in 3-degree increments in order to reduce any random errors and the size of the density data set without degrading the quality (Sutton, 2011a, 2011b). Density data with uncertainties exceeding two standard deviations are excluded to avoid highly deviated data.

The TIMED-GUVI satellite provided the limb scan measurements of airglow on the dayside from 12:00 to 16:00 LT during the November 2003 storm period. The major neutral compositions (O, O_2, and N_2) are calculated from the UV radiance of the different colors/wavelength bands: OI 135.6 nm and Lyman-Birge-Hopfield (LBH) 140–180 nm (Christensen et al., 2003; Emmert et al., 2006; Paxton et al., 1999). The retrieval algorithms are similar to those used for SSUSI (Special Sensor UV Spectrographic Imager) (Paxton et al., 1998). The Level 1B airglow data are inverted into the neutral density profiles (Level 2B) from March 2002 to August 2007 (http://guvitimed.jhuapl.edu/data_products). Retrievals used in this study are based on data collected at solar zenith angles (SZA) less than 60° and latitudes below 80°. There is a minor systematic issue beyond 70°–75° SZA that appears to be related to the loss of sensitivity to molecular species at large SZA. The most reliable data are obtained with SZA < 60°, except for atomic oxygen, which is accurate to 70° or larger (see http://guvitimed.jhuapl.edu/sites/default/files/data/documents/readme_GUVI_Version_13_Limb_Retrievals.pdf for more details). Thus, in this study, the neutral density and compositions beyond 60° SZA are excluded.

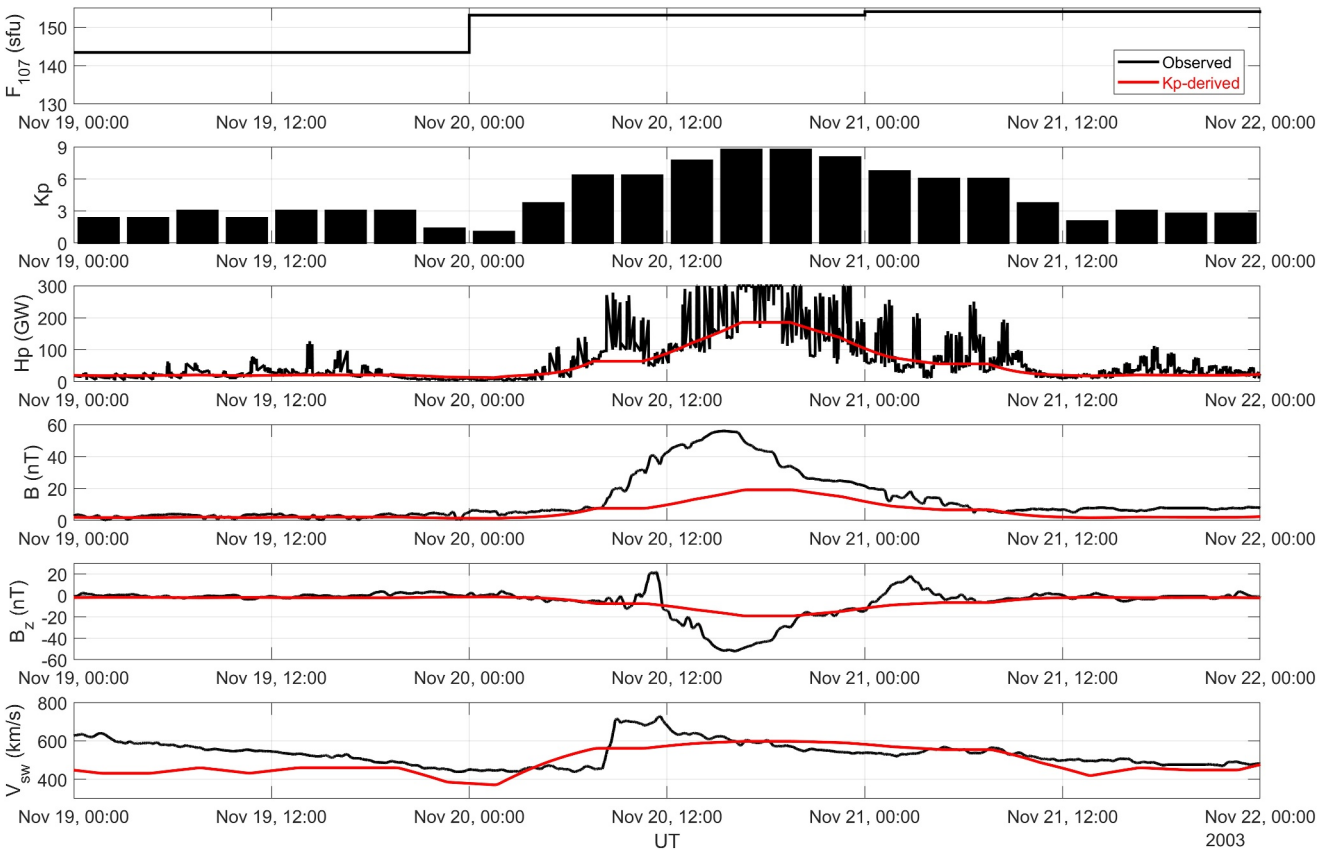

Figure 1. An overview plot of observed (black lines and bars) and Kp-derived (red lines) $F_{10.7}$, Kp, Hp, and solar wind parameters during 19–21 November 2003.

3. Results

Figure 1 displays the observed solar and geomagnetic parameters during the storm period of 19–21 November. A modest increase of $F_{10.7}$ from 143 to 153 sfu was observed over the course of the first two days. Geomagnetic activity, as indicated by the Kp index, started to increase early on 20 November, together with increased Hp/IMF B/V_{sw} and decreased IMF B_z. Kp index returned back to quiet levels below 3 by 12:00 UT on 21 November. A dramatic change of Hp from ∼7 to 300 GW was seen from 03:30 to 14:00 UT on 20 November, which indicates increasing auroral precipitation and polar cap potential (Foster et al., 1986). It returned to the low value of ∼10 GW at 11:00 UT on 21 November. V_{sw} increased from 455 km/s around 08:00 UT to 713 km/s at 08:55 UT on 20 November, and subsequently, returned to pre-storm levels around 500 km/s at 11:00 UT on 21 November. IMF B began to increase at around 08:00 UT and reached its maximum of 56 nT at 15:27 UT on 20 November, and the enhancement lasted for 15 hr until it returned to pre-storm levels around 6 nT at 06:30 UT on 21 November. IMF B_z turned negative at ∼11:30 UT, and yielded a minimum of −52 nT at 16:08 UT. The negative B_z value lasted for almost 14 hr (from 11:30 UT on 20 November to 01:00 UT on the 21 November). The IMF orientation has an important influence on the magnetosphere and high-latitude ionosphere with more negative IMF B_z resulting in pronounced effects on the upper atmosphere (Davis et al., 1997). In general, these parameters suggest that the storm began affecting the Earth's magnetosphere after 03:00 UT on 20 November, becoming most intense at 14:00–16:00 UT on 20 November, with sustained activity until around 12:00 UT on 21 November. Figure 1 also shows the solar wind/IMF and Hp conditions derived from empirical relationships currently used in the operational WAM-IPE. It can be seen these estimates are significantly lower than the observed values. Table 1 illustrates the empirical formulas of Kp and the associated Kp-derived solar parameters which serve as external drivers in WAM. Table 1 was derived based on a statistical relationship between Kp from 1 to 9 and observed solar wind parameters, Hp and IMF B_z from the NASA Advanced Composition Explorer satellite since 1998. Figure 2 displays the temporal evolution of thermospheric mass density from the WAM free run, CHAMP observations, and IDEA based on the setup in Sutton (2018). The heavy lines depict the neutral density average of 3

Table 1
Equations of Solar Parameters in Whole Atmosphere Model

Solar parameter	Equation	Value at Kp = 9
Hp (GW)	$1.29 + 15.60\text{Kp} - 4.93\text{Kp}^2 + 0.64\text{Kp}^3$	208.92
IMF B (nT)	$\sqrt{\text{IMF } B_z{}^2 + \text{IMF } B_y{}^2}$	21.27
IMF B_z (nT)	$\frac{-E_{sw} \times 1000}{V_{sw}}$	−21.27
V_{sw} (km/s)	$317.0 + 55.84\text{Kp} - 2.71\text{Kp}^2$	600.00
E_{sw} (mV/m)	$0.1455 + 0.4675\text{kp} - 0.1446\text{kp}^2 + 0.0276\text{kp}^3$	12.76

Note. IMF B_y is assumed to be 0.

CHAMP orbits (i.e., approximately 4.5 hr) using a moving window of 1.5 hr, and the thinner lines the density values at the satellite location along the orbit. Note that the observed quiet-time neutral density values along the orbit are sampling the global diurnal/latitude neutral density structure, which are well captured by the physical model driven by observed and Kp-derived parameters aside from a model bias of about 30% and 10%, respectively, that persists throughout this quiet period. The WAM model driven by observed solar wind/IMF drivers actually captures the response seen by CHAMP very well. However, that is most likely not always the case, which is why a data assimilation is being investigated for cases that are not so close. The WAM neutral density increases during the storm using the Kp derived drivers appears to be significantly lower than the WAM density using the observed drivers, which can be attributed to the fact that (a) the derived V_{sw}, IMF B/B_z, and Hp generally underestimate the observed values (Figure 1), and (b) the time variability of the derived drivers is lower than that of the observed drivers. Figure 2 reveals that the CHAMP density reached its maximum at 21:45 UT, while WAM with observed and Kp-derived drivers peaked earlier at 20:15 UT, yielding a 90-min time delay. The time delay in the occurrence of the density peak and the underestimation of the density value between CHAMP and WAM with observed and Kp-derived drivers indicate that improvement in the model prediction is needed. After applying the

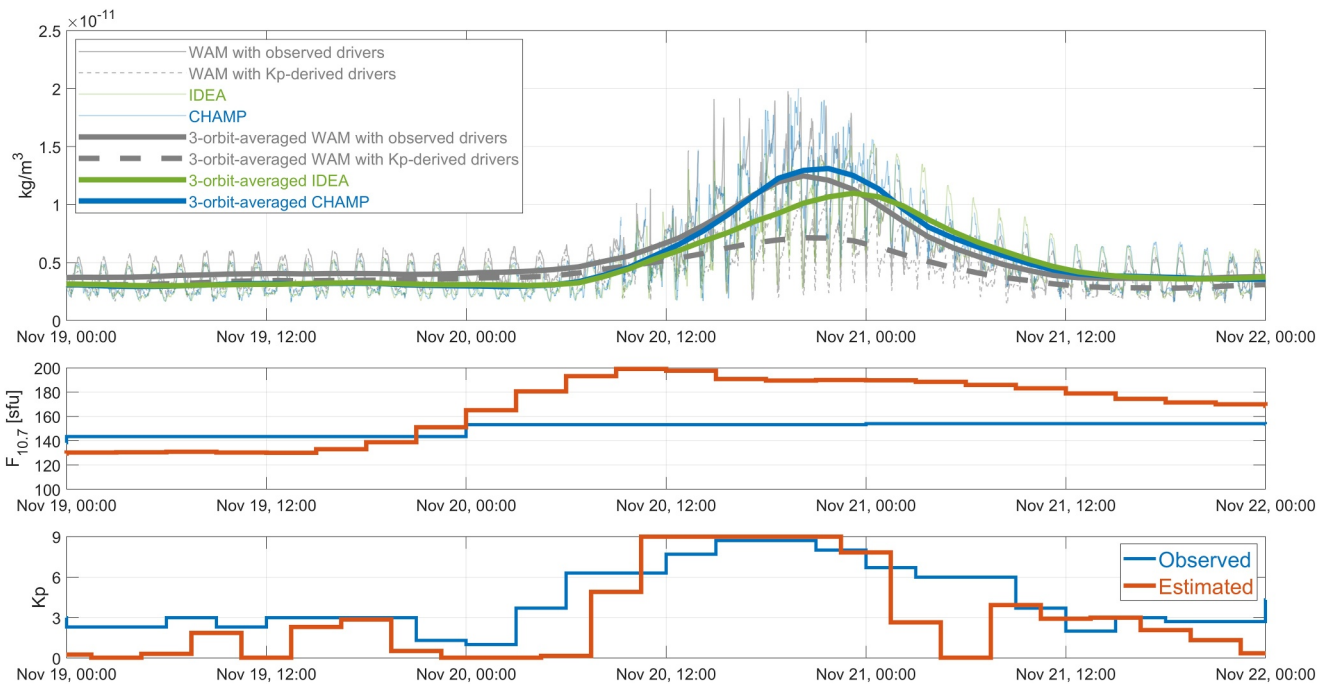

Figure 2. Time evolution of the neutral mass density obtained from Challenging Mini-Satellite Payload (CHAMP) observations (blue solid line), Whole Atmosphere Model (WAM) free run with observed SW drivers (gray solid line), WAM free run with Kp-derived SW drivers (gray dashed line), and Iterative Driver Estimation and Assimilation (IDEA) data assimilation with old WAM drivers (light green solid line). Thinner lines represent raw data of the data set mentioned above along the CHAMP satellite orbit. Thicker lines stand for their averages of 3 CHAMP orbits (i.e., about 4.5 hr) with a moving window of 1.5 hr. Bottom panels are observed $F_{10.7}$ and Kp (blue lines) and $F_{10.7}$ and Kp estimates for IDEA. Note that the $F_{10.7}$ and Kp estimates are constant for 3 hr at a time.

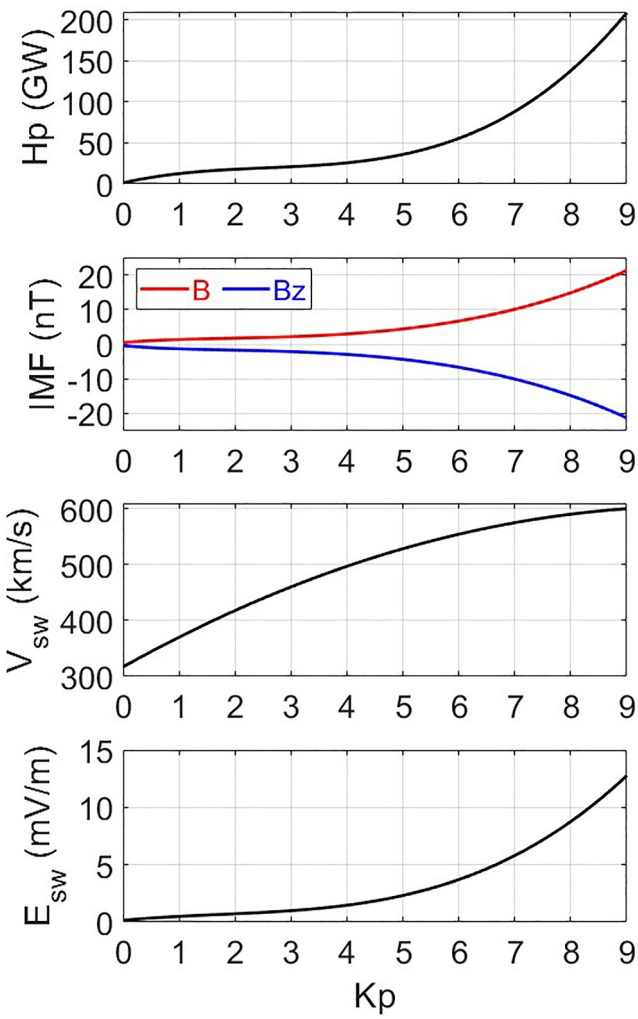

Figure 3. The relationships used in the Kp-derived Whole Atmosphere Model free runs to calculate solar wind conditions from Kp. These are typically used in forecast mode, when forecasts of Kp are available but solar wind conditions are not.

IDEA technique, Figure 2 shows that the estimated Kp reached the maximum of 9 during 10:00–19:00 UT on 20 November, but the model was still not able to reach the high levels of the observed density, since the original empirical relationship of Kp with solar wind/IMF delivers insufficient energy and heating to the thermospheric system. To make up for the density discrepancy, IDEA enhanced the $F_{10.7}$ value; however, the response of the modeled neutral density to the enhanced $F_{10.7}$ value was not strong enough to capture the observed increase in CHAMP density. As a result, the WAM density was not capable of capturing the CHAMP density until approximately 02:00 UT on 21 November, after the recovery phase had begun. Figure 3 depicts the relationship between Kp and these parameters based on the formulas shown in Table 1. Owing to the Kp scale being capped at 9, the related derived external solar drivers were limited by these empirical relationships, which tend to underestimate the observed values (Figure 1). To rectify this problem, several changes were made to WAM's external drivers. The first was allowing the Kp scale to exceed 9. In Sutton (2018), any Kp estimated more than 9 would be replaced with 9. In this study, we simply removed this process in the IDEA estimation procedure to allow the estimated Kp to exceed beyond 9. During the IDEA data assimilation process, the estimated $F_{10.7}$ and Kp serve to correct model errors and to minimize the model variance. In order to minimize the model errors, Kp is allowed to exceed beyond 9, and therefore, the associated Kp-derived parameters can be further enhanced to adjust the model output appropriately. The second was changing the relationship between Kp and V_{sw}. Extracting from Table 1, the original equation of V_{sw} is given by,

$$V_{sw} = 317 + 55.84\text{Kp} - 2.71\text{Kp}^2 \quad (1)$$

Equation 1 was derived based on a statistical relationship between Kp from 1 to 9 and observed solar wind values of velocity and IMF B_z. Since the fit was limited to Kp at 9, it was a good fit within this range. According to Equation 1, V_{sw} steadily increases and reaches its maximum of 604.6 km/s at Kp = 10.3 and decreases afterward. This decrease at larger Kp values, is an artifact of the analytical fit and does not allow WAM to attain adequately high densities, especially for extreme storm cases when the effective Kp may be higher than 9. To address this issue, a new relationship for V_{sw} was implemented by adjusting the second and third coefficients in Equation 1:

$$V_{sw} = 317 + 47.13\text{Kp} - 1.36\text{Kp}^2 \quad (2)$$

Figure 4a displays a comparison of the two equations for V_{sw}. The purpose of Equation 2 is to maintain V_{sw} values similar to those in Equation 1 up to Kp ~ 6, while it continues to increase up to 725.3 km/s at Kp = 17.3. The solar wind velocity of 725.3 km/s was a reasonable value in comparison to the observed ones (Figure 1). Figure 4a shows that Equation 2 is a better relationship for V_{sw} when applying the IDEA technique. Figure 4b illustrates that Equation 2 effectively enhanced the density outputs around 15:00–19:00 UT on 20 November when Kp = 9. This improvement would be more significant when the IDEA-estimated Kp exceed 9.

Figure 5 exhibits the temporal evolution of the thermospheric neutral mass density obtained from CHAMP, WAM free runs, and the IDEA data assimilation with the adjustments mentioned above (referred to as "IDEA with adjusted WAM drivers" hereafter) during 19–21 November 2003. Figure 5 shows that the IDEA data assimilation method has effectively improved the neutral density nowcast with only −5.3% bias relative to CHAMP during the storm time period of 20 November. During the recovery phase on 21 November, WAM runs with observed and Kp-derived drivers were consistently lower than CHAMP, while IDEA effectively captured the CHAMP density enhancements. Table 2 displays bias, RMSe, and standard deviation (STD) for the CHAMP log density and its 3-orbit average with respect to four density outputs: free-running WAMs with observed and Kp-derived drivers and IDEA outputs with old and adjusted WAM drivers during the storm period from 20 to 21 November. Given that

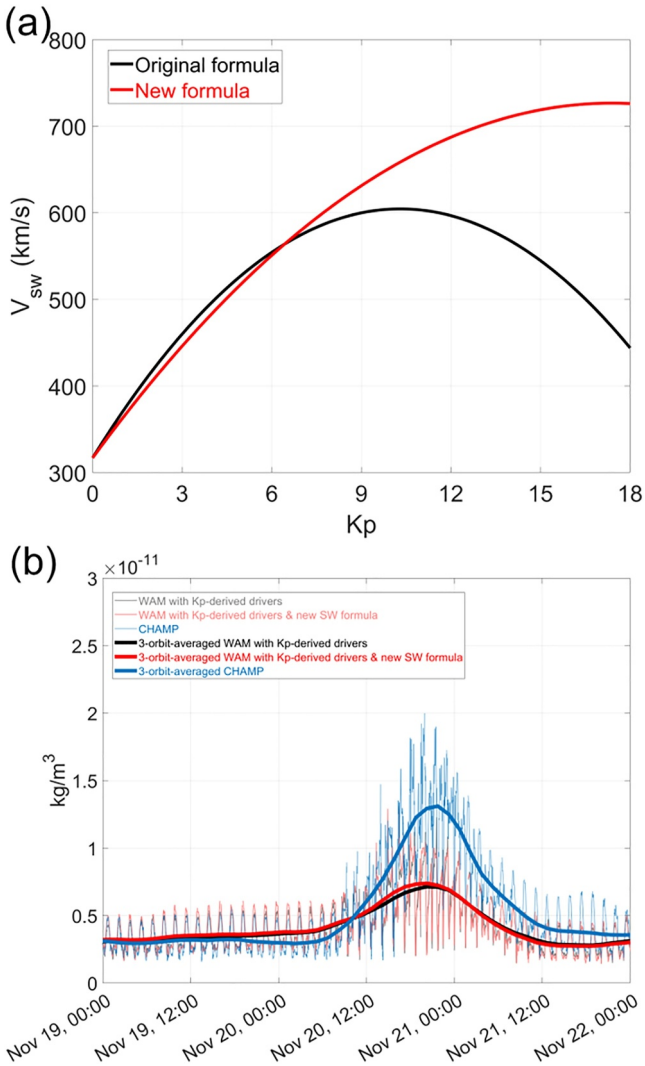

Figure 4. A comparison of (a) relationships between Kp and V_{sw} using Equation 1 (black curve) and Equation 2 (red curve) and (b) neutral densities of free-running Whole Atmosphere Model using Equation 1 (black curve) and Equation 2 (red curve) and Challenging Mini-Satellite Payload observations (blue curve).

the IDEA system minimizes the RMSe in the log densities, the bias, RMSe, and STD are calculated in log space (Sutton, 2018), and the quantities are expressed as percentages, for example, % = 100 × (exp(RMSe) − 1). Note that "IDEA with old WAM drivers" refers to the IDEA output shown in Figure 2. From the 3-orbit-averaged perspective, IDEA with adjusted WAM drivers clearly outperforms free-running WAMs and IDEA with old WAM drivers. On the other hand, along CHAMP orbits, IDEA with adjusted WAM drivers exhibits better performance compared to free-running WAMs and slightly outperforms IDEA with old WAM drivers.

Figure 6 illustrates the time variation of RMSe in free-running WAM with observed and Kp-derived drivers and IDEA with adjusted WAM drivers in comparison to CHAMP from the 3-orbit-averaged perspective. The free-running WAM with observed drivers exhibits a large RMSe about 20%–35% on 19 November, but the value decreased to 5%–13% on 20 November and sustained until 22 November. In contrast, the free-running WAM with Kp-derived drivers displays a low RMSe of 6%–10% for the first 12 hr of 19 November, while it began to enhance up to 70% around 00:00 UT 21 November. On the other hand, RMSe of IDEA with adjusted WAM drivers reduced considerably to below 8% throughout the period of 19–21 November. The RMSe of IDEA with adjusted WAM drivers was fairly low with respect to the two WAM free runs and rarely exceeded 6% on the quiet day of 19 November and in the recovery phase on 21 November. Figure 6 shows that IDEA has effectively reduced the RMSe during both quiet and geomagnetic disturbed days, which indicates the usefulness of the IDEA technique in improving the predictive capability for neutral density.

4. Discussion

One prominent discrepancy, however, between WAM and CHAMP densities in Figure 5 is the occurrence of low-density features in WAM from 16:00 to 22:00 UT on 20 November. These low-density features are only present during the storm time period. Figure 7 focuses on the neutral density from 12:00 to 22:00 UT on 20 November along the CHAMP satellite orbit. The prominent density dip feature can be seen in CHAMP, WAM free runs, and IDEA with adjusted WAM drivers repeatedly during the early phase of the storm from 12:00 to 16:00 UT. However, while this feature remained present in WAM free runs and IDEA with adjusted WAM drivers during the peak of the storm from 16:00 to 22:00 UT, it was absent from CHAMP observations. The middle and bottom panels of Figure 7 illustrate that these density dips occurred repeatedly in the high-latitude regions of both hemispheres, mostly on the nightside of the noon-midnight orbit. Here, we focused on two cases around 12:35 and 20:12 UT. Figure 8a presents a snapshot of the polar plot in the southern hemisphere from 30°S to 90°S at 12:30 UT and time variation of the neutral density from 12:20 to 12:50 UT. Both the model and CHAMP displayed a density minimum at 12:33 and 12:35 UT, respectively. The former minimum corresponds to the density hole in WAM within 60°S–90°S on the nightside. The model and CHAMP generally exhibited similar features and patterns in neutral density during this period, and this consistency was seen from 12:00 to 16:00 UT. This density hole structure has been widely investigated over decades (e.g., Fuller-Rowell et al., 1999; Schlegel et al., 2005; Schoendorf, Crowley, Roble, & Marcos, 1996, Schoendorf, Crowley, & Roble, 1996). Fuller-Rowell et al. (1999) found that these density holes are dynamically driven, created by the high-velocity neutral winds from ion drag which are usually seen during strong geomagnetic activity. On the other hand, Figure 8b displays another snapshot of the polar plot, along with the time variation of the neutral density in the model and CHAMP from 20:00 to 20:30 UT. A significant density hole formed in 60°S–90°S several hours after midnight, while the CHAMP satellite passed through this region and did not observe the associated density minimum. Comparing Figures 8a and 8b, we find that the density hole feature is

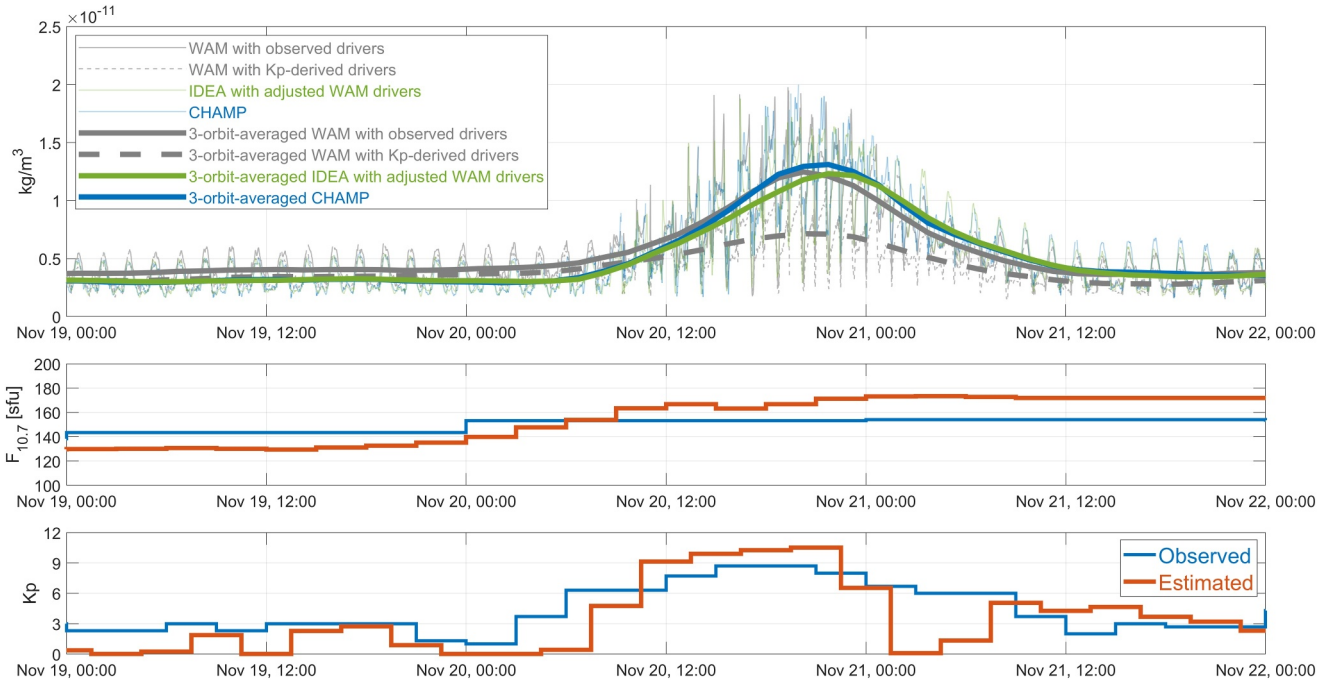

Figure 5. Similar to Figure 2 but the Iterative Driver Estimation and Assimilation output is obtained with adjusted Whole Atmosphere Model drivers.

well captured by the model, while its real location may deviate from the CHAMP satellite location, resulting in the underestimated WAM density seen during the storm period of 16:00–22:00 UT.

In addition to different locations in anomalous density dips between observed and modeled neutral densities, we speculate that the 3-hr advancement of the data assimilation window could also cause the density discrepancy as it may not be sufficient to capture some of the rapid changes in the thermosphere during extreme storm periods. Therefore, we attempt to experiment whether changing the data assimilation window improves model-data agreement. Figure 9 exhibits the IDEA outputs with a halving Kp estimation time window (i.e., 1.5 hr). Moreover, the $F_{10.7}$ estimation time window remains unchanged at 24 hr in order to limit the correlation between Kp and $F_{10.7}$ corrections. This means that the six latest 1.5-hr Kp indices, together with a 1-day effective $F_{10.7}$, are now estimated for a total of seven quantities during each data assimilation step. Figure 9 shows that IDEA with adjusted Kp/$F_{10.7}$ windows has improved the rise time of densities on 20 November. Table 2 presents bias, RMSe, and STD of IDEA with adjusted Kp/$F_{10.7}$ windows relative to CHAMP. It can be seen that, while bias is smaller, RMSe and STD of IDEA with adjusted Kp/$F_{10.7}$ windows are larger than IDEA with adjusted WAM drivers. This indicates that changing the data assimilation window has effectively improved the model-data agreement in terms of bias, while RMSe and STD being worse indicates that the observability become poor when estimating six 1.5-hr Kp values.

The IDEA data assimilation system uses CHAMP neutral density estimates from accelerometer measurements in the present study. For future operational configurations of neutral density data assimilation in WAM it is useful to

Table 2
Performance Metrics of Whole Atmosphere Model Neutral Density Relative to Challenging Mini-Satellite Payload Measurements During 20–21 November

	Bias		RMSe		STD	
	Along-orbit (%)	3-Orbit-average (%)	Along-orbit (%)	3-Orbit-average (%)	Along-orbit (%)	3-Orbit-average (%)
WAM with observed drivers	4.5	3.4	32.9	18.2	32.4	17.8
WAM with Kp-derived drivers	−21.4	−22.4	53.9	44.5	42.9	30.5
IDEA with old WAM drivers	−5.3	−3.4	25.4	11.2	24.6	10.5
IDEA with adjusted WAM drivers	−4.1	−2.3	23.5	5.2	23.0	4.6
IDEA with adjusted Kp/$F_{10.7}$ windows	−2.4	−1.1	24.4	5.8	24.3	5.7

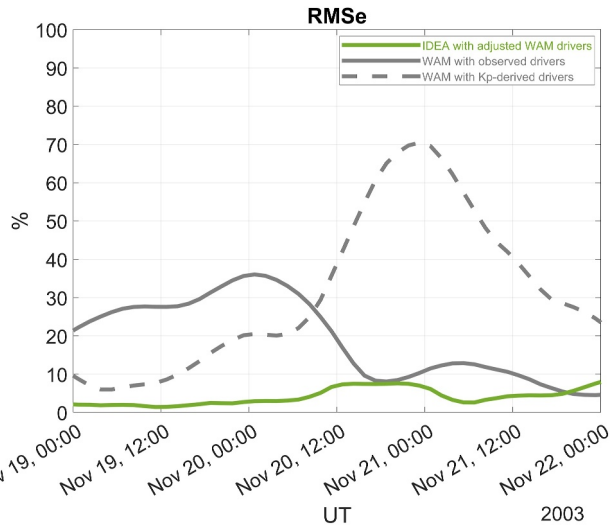

Figure 6. Root-mean-square errors of observed/Kp-derived drivers Whole Atmosphere Model free runs and Iterative Driver Estimation and Assimilation neutral density with respect to 3-orbital-averaged Challenging Mini-Satellite Payload observations.

explore alternative data sources. One such data source is the neutral density estimated from GUVI airglow observations. We compared the data set of GUVI neutral density retrieved from airglow observations with the IDEA densities adjusted by assimilating CHAMP. Here, we used IDEA outputs with adjusted WAM drivers for two reasons: the IDEA technique aims to minimize the RMSe of log density between a model and observed data (Sutton, 2018), and Table 2 shows that IDEA with adjusted Kp/$F_{10.7}$ windows yields the least RMSe. Free-running WAMs with observed and Kp-derived drivers were also compared to demonstrate how much the IDEA improves the neutral density outputs relative to the free-running WAMs in comparison to the GUVI neutral density observations. It should be noticed that neutral density estimates obtained from GUVI measurements are available only during the daytime from 12:00 to 16:00 LT. GUVI neutral density profiles are interpolated along the altitude with a 10 km resolution. Figure 10 displays bias, RMSe, and STD of GUVI versus IDEA and the free-running WAMs along altitudes of 110–500 km with a 10 km interval over the time period of 19–21 November 2003. Figure 10 demonstrates that assimilation of CHAMP observations in IDEA had effectively improved the neutral density outputs in comparison to the independent measurements of GUVI neutral densities. From the 3-orbit-averaged perspective, for example, RMSe and STD in GUVI versus IDEA are lower than 10% at the altitude within 210–370 km, while those in GUVI versus free-running WAMs with observed and Kp-derived drivers are generally higher than 10% and 15%, respectively. The bias of the along-orbit data and the 3-orbit average between GUVI and IDEA approaches 0 at the altitude of 320 km. The RMSe values are at their minimum values at 290 and 300 km, respectively, and the STD values are lowest at altitudes of 270 and 280 km, respectively. In general, this shows that GUVI limb scan measurements are the most consistent with CHAMP and IDEA at altitudes ranging from 270 to 320 km. Figure 11 displays the temporal evolution of IDEA and GUVI densities at 300 km altitude

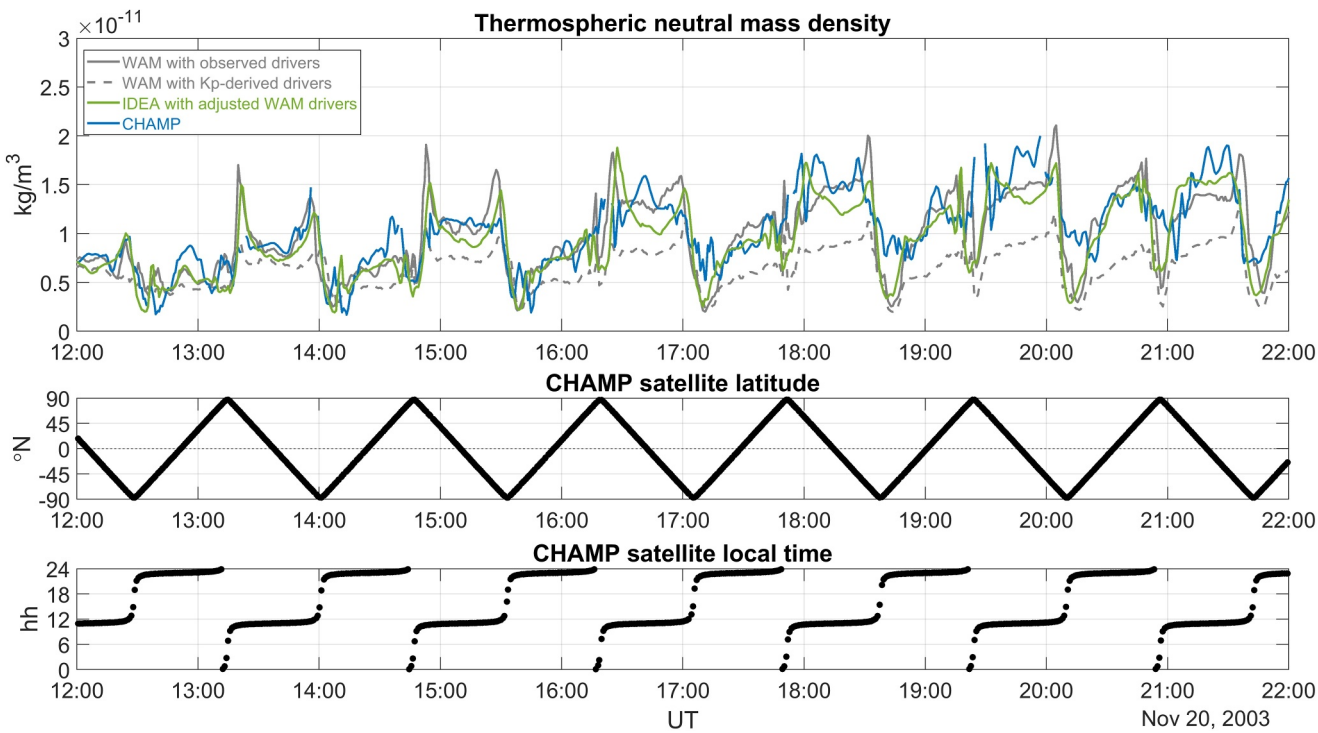

Figure 7. (top) Similar to Figure 5 but for 12:00–22:00 UT on 20 November 2003. (mid) Challenging Mini-Satellite Payload (CHAMP) satellite locations in latitude. (bottom) CHAMP satellite local time. Red lines denote the density dip in CHAMP near 12:35 UT and that in Iterative Driver Estimation and Assimilation near 20:12 UT.

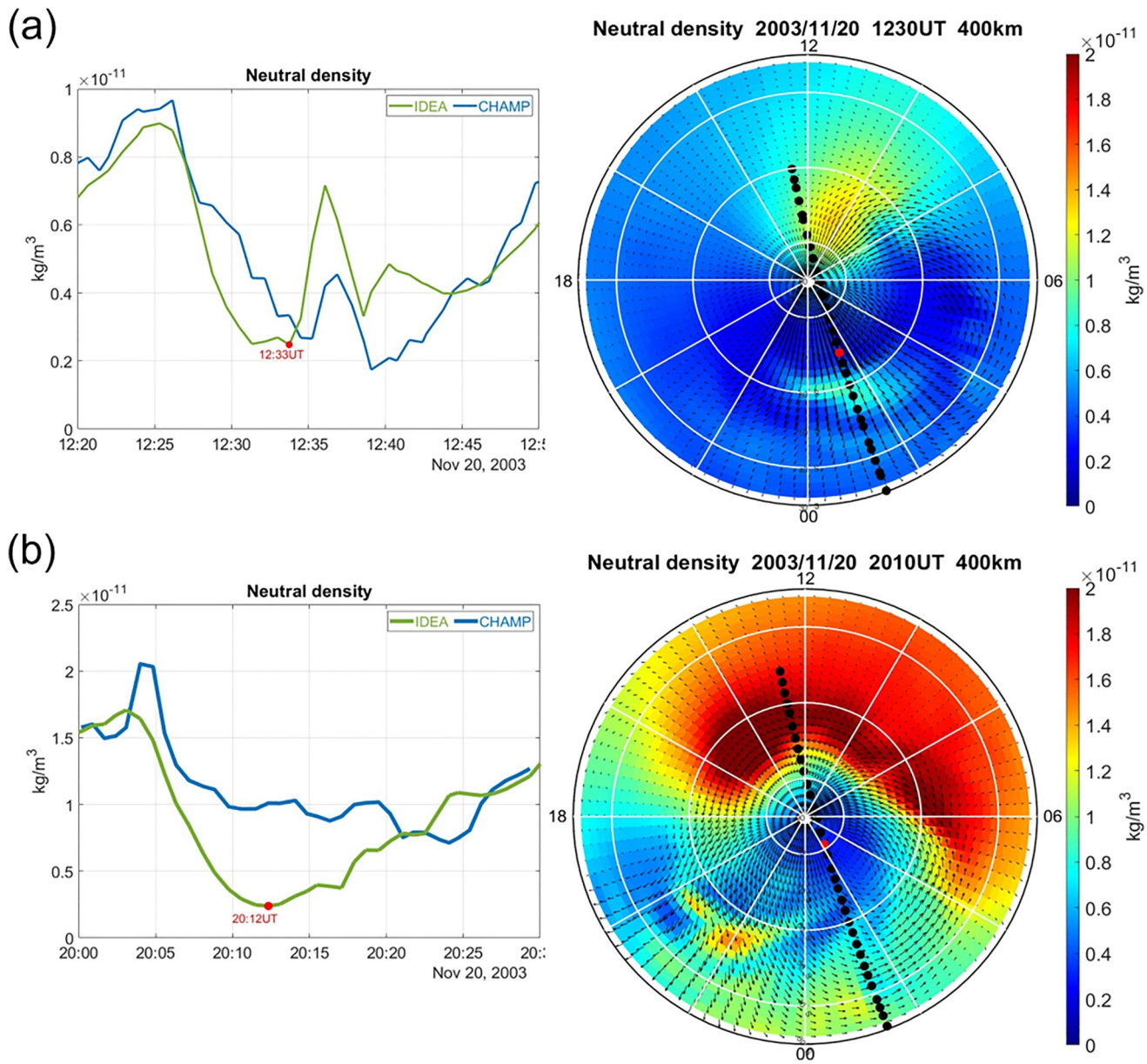

Figure 8. Left columns show Iterative Driver Estimation and Assimilation (IDEA) with adjusted Whole Atmosphere Model drivers and Challenging Mini-Satellite Payload (CHAMP) neutral density sampled along the CHAMP orbit. Right columns show snapshots of IDEA neutral density at 400 km in 30°S–90°S. (a) 12:20–12:50 UT (12:30 UT for the snapshot) and (b) 20:00–20:30 UT (20:10 UT for the snapshot). Red dots in the figures indicate a density minimum in IDEA and the corresponding CHAMP satellite location.

during the period of 19–21 November 2003. Outliers in the GUVI data, along with corresponding model outputs near 00:00 UT on 21 November are discarded. GUVI data exhibit more fluctuations compared to model output, possibly due to systematic biases and inversion algorithm assumptions degrading at high latitudes and/or regions of large solar zenith angle. Nonetheless, a bias of 1.0%, RMSe of 13.5%, and STD of 13.5% between GUVI and IDEA along the GUVI orbits are lower than the corresponding values of −4.1%, 23.5%, and 23.0% between CHAMP and IDEA with adjusted WAM drivers (Table 2). In addition, the 3-orbit-averaged values also show strong agreement, with bias, RMSe, and STD of 1.0%, 5.6%, and 5.6%, respectively, which are comparable to the corresponding values of −2.3%, 5.2%, and 4.6% between CHAMP and IDEA with adjusted WAM drivers (Table 2) during the storm period of 20–21 November 2003. Figure 11 also shows that IDEA displays a closer agreement with GUVI densities than free-running WAMs throughout the storm period. These results demonstrate

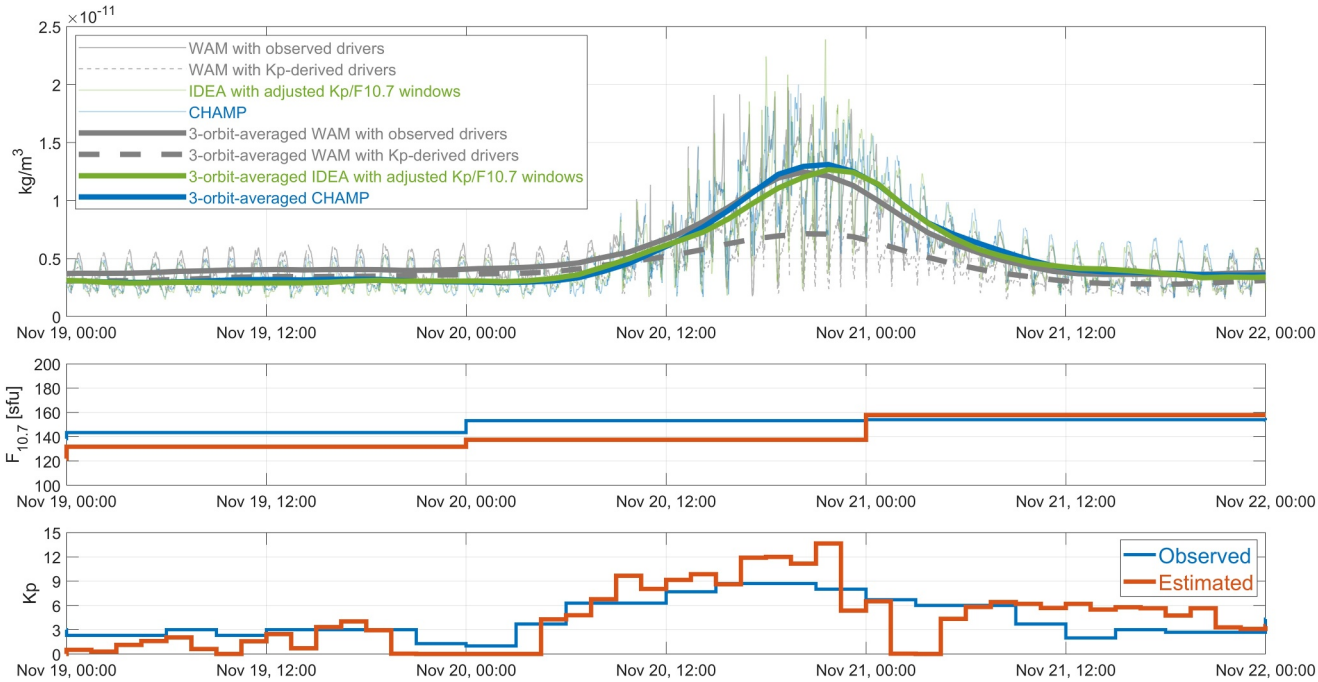

Figure 9. Similar to Figure 5 but the Kp estimation windows are adjusted from 3 to 1.5 hr and $F_{10.7}$ remains unchanged at 24 hr.

the potential utility of using GUVI limb scan measurements as the data source in the IDEA data assimilation system.

5. Conclusion

The IDEA data assimilation technique significantly improves the nowcasting capabilities of WAM thermospheric neutral densities during the extreme geomagnetic storm in November 2003 by iteratively tuning the $F_{10.7}$ and Kp index. Due to the intensity of the storm, a number of adjustments were made to WAM. The first was having an open-ended Kp scale in the estimation procedure, which allowed for extended estimates of energy input from the solar wind and IMF, effectively increasing the neutral density. The second was changing the relationship between Kp and solar wind velocity. With modified coefficients, the solar wind velocity increased more realistically as the Kp scale grew. The new equation ensures that neutral density increases when the estimated Kp index previously became saturated at a value of 9. With these changes, results show that the RMSe of IDEA output with respect to CHAMP density was consistently below 8% during both geomagnetically quiet and disturbed days, while the free-running WAM with observed and Kp-derived SW drivers yielded greater RMSe values with maximums of about 35% and 70%, respectively. Additionally, we experimented with a decreased the Kp estimation window from 3 to 1.5 hr, without changing the 1-day effective $F_{10.7}$ estimate window. The reduced Kp window effectively captures more rapid changes in the thermospheric states during a storm, while the use of the 1-day $F_{10.7}$ estimate reduced the correlation between Kp and F10.7 estimates. However, changing the windows resulted in poor observability when estimating six 1.5-hr Kp values, which in turn led to worse RMSe and STD. Overall, IDEA with adjusted WAM drivers effectively improved data-model agreement, with a bias of −2.3%, RMSe of 5.2%, and STD of 4.6%, between IDEA and CHAMP 3-orbital-averaged neutral log densities throughout the storm period.

The main discrepancy between the model and CHAMP densities during the peak of the storm is due to differences in anomalous density dips. These density anomalies are present in both the free-running WAM and IDEA output, as well as in the CHAMP data itself. However, this discrepancy could be explained by the model not being able to accurately locate the density hole features over the polar regions. The density anomalies in the model outputs were prominent during the storm, while rather insignificant in the quiet time. In contrast, the density anomalies in

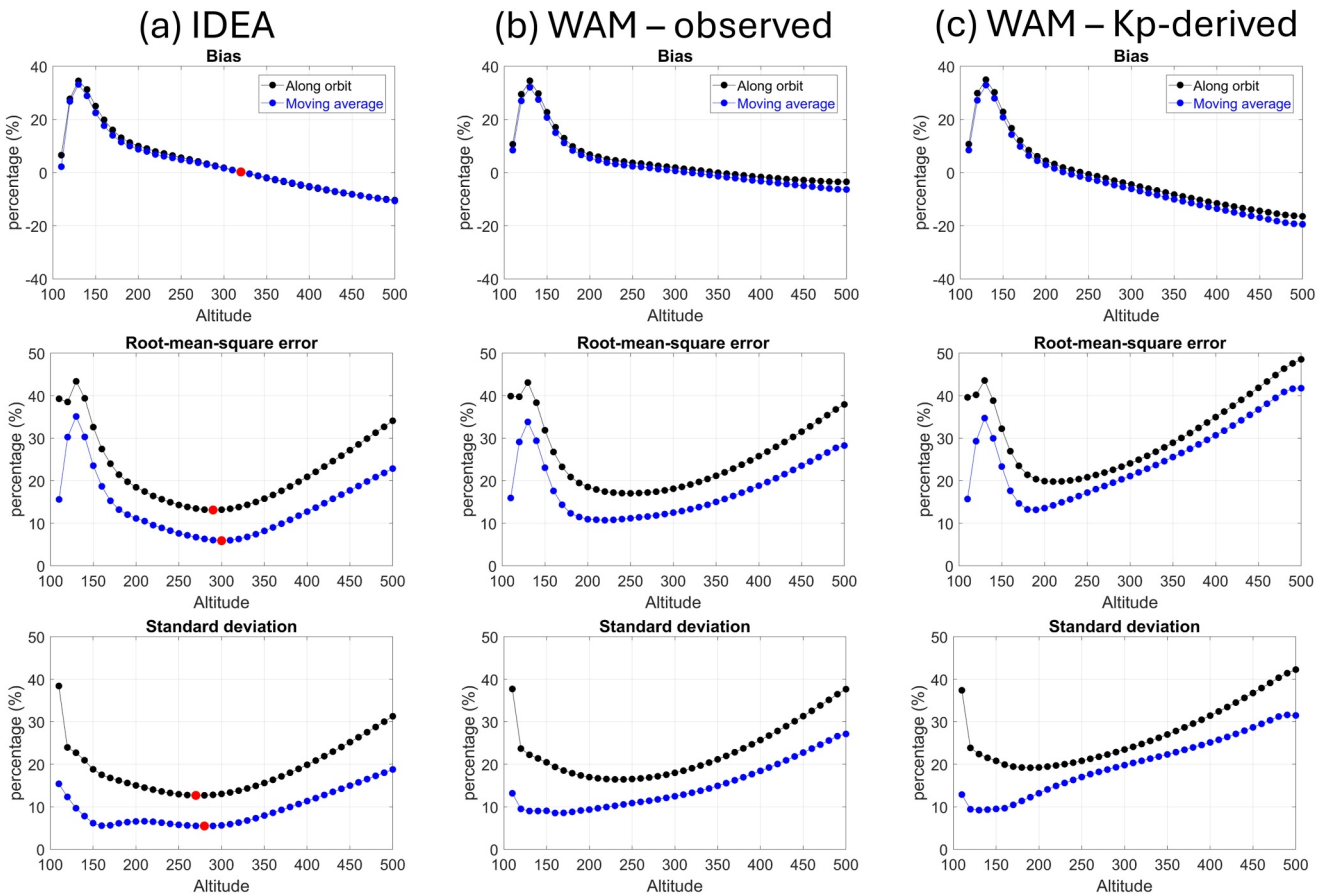

Figure 10. Performance metrics of Global Ultraviolet Imager with respect to (a) Iterative Driver Estimation and Assimilation neutral density, (b) Whole Atmosphere Model (WAM) with observed drivers, and (c) WAM with Kp-derived drivers at various altitudes during the period of 19–21 November 2003. Red dots in panel (a) denoted in the figure highlight when the bias is closest to 0 and when minimum values of root-mean-square error and standard deviation are reached.

CHAMP can only be seen during 12:00–16:00 UT on 20 November. To solve this problem, further investigation and improvement of the modeling technique is required in the future.

In order to validate the IDEA output and explore alternative data sources to be assimilated, IDEA neutral density output was cross-compared with TIMED-GUVI dayside limb scan measurements. Compared with model free runs, IDEA yielded smaller RMSe and STD values against GUVI neutral densities. Results show good agreement between IDEA and GUVI neutral densities at altitudes of 270–320 km, with a RMSe values of 13.5% for densities and 5.6% for 3-orbital averaged densities at 300 km. The good agreement demonstrates the potential of instruments similar to TIMED-GUVI limb scan in improving WAM thermospheric neutral density nowcast and forecast systems. Given the fact that neutral density estimates from TIMED-GUVI limb scan measurements are available only during daytime, they may be able to be used simultaneously with another data type (e.g., accelerometer) to supplement the information. Strong variations in the neutral density of the thermosphere heavily impact the position of LEO objects as they respond to radiative inputs from the Sun, auroral activity, and electrical currents generated during a geomagnetic storm. Therefore, the improved neutral density specification in the IDEA scheme presented can significantly benefit the ability to track and predict the trajectories of low Earth orbiting satellites, and exploration of possible data sources such as TIMED-GUVI limb scan measurements could be of value to the future operational configuration of IDEA data assimilation with WAM.

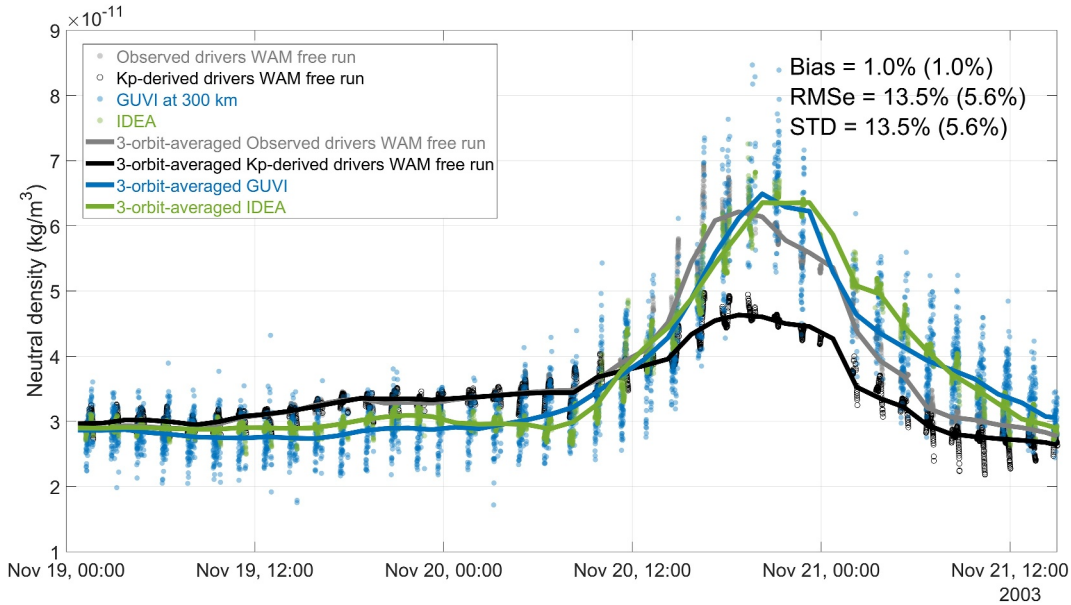

Figure 11. Comparison of Global Ultraviolet Imager (GUVI) versus Iterative Driver Estimation and Assimilation, Whole Atmosphere Model (WAM) with observed drivers, and WAM with Kp-derived drivers neutral density. Black circle, light green, light blue, and gray dots stand for neutral densities sampled along the Thermosphere Ionosphere Mesosphere Energetics and Dynamics/GUVI limb scan tangent point, while gray, black, blue, and green solid lines represent the associated 3-orbit-average values.

Data Availability Statement

The CHAMP accelerometer estimates of neutral density is publicly accessible at https://zenodo.org/doi/10.5281/zenodo.13287613 (Sutton, 2011a, 2011b). The TIMED/GUVI limb-scan measurements and retrieved neutral density profiles are publicly available at https://guvitimed.jhuapl.edu/data_fetch_l2b_ndp_idlsave (TIMED/GUVI, 2014).

Acknowledgments

Ching-Chung Cheng, Timothy J. Fuller-Rowell, and Eric Sutton were supported by NSF Space Weather with Quantification of Uncertainties program under Grant AGS 2028032. Eric Sutton was also supported by the NASA SWO2R program under Grant 80NSSC20K1399. Jenn-Yenq Liu was supported by the National Science and Technology Council (NSTC) Grant NSTC 112-2123-M-008-003. This material is based upon work supported by the NSF National Center for Atmospheric Research, which is a major facility sponsored by the U.S. National Science Foundation under Cooperative Agreement 1852977. High-performance computing support from Cheyenne and Derecho was provided by NCAR's Computational and Information Systems Laboratory. The source code for WAM-IPE can be downloaded at the following GitHub repository (https://github.com/CU-SWQU/GSMWAM-IPE).

References

Akmaev, R. A. (2001). Simulation of large-scale dynamics in the mesosphere and lower thermosphere with the Doppler-spread parameterization of gravity waves: 1. Implementation and zonal mean climatologies. *Journal of Geophysical Research*, *106*(D1), 1193–1204. https://doi.org/10.1029/2000jd900520

Akmaev, R. A., Fuller-Rowell, T. J., Wu, F., Forbes, J. M., Zhang, X., Anghel, A. F., et al. (2008). Tidal variability in the lower thermosphere: Comparison of Whole Atmosphere Model (WAM) simulations with observations from TIMED. *Geophysical Research Letters*, *35*(3), L03810. https://doi.org/10.1029/2007GL032584

Berger, T. E., Holzinger, M. J., Sutton, E. K., & Thayer, J. P. (2020). Flying through uncertainty. *Space Weather*, *18*(1), e2019SW002373. https://doi.org/10.1029/2019SW002373

Bortnik, J., Thorne, R. M., O'Brien, T. P., Green, J. C., Strangeway, R. J., Shprits, Y. Y., & Baker, D. N. (2006). Observation of two distinct, rapid loss mechanisms during the 20 November 2003 radiation belt dropout event. *Journal of Geophysical Research*, *111*(A12), A12216. https://doi.org/10.1029/2006JA011802

Bruinsma, S., Forbes, J. M., Nerem, R. S., & Zhang, X. (2006). Thermosphere density response to the 20–21 November 2003 solar and geomagnetic storm from CHAMP and GRACE accelerometer data. *Journal of Geophysical Research*, *111*(A6), A06303. https://doi.org/10.1029/2005JA011284

Bruinsma, S., Tamagnan, D., & Biancale, R. (2004). Atmospheric densities derived from CHAMP/STAR accelerometer observations. *Planetary and Space Science*, *52*(4), 297–312. https://doi.org/10.1016/j.pss.2003.11.004

Cantrall, C. E., Matsuo, T., & Solomon, S. C. (2019). Upper atmosphere radiance data assimilation: A feasibility study for gold far ultraviolet observations. *Journal of Geophysical Research: Space Physics*, *124*(10), 8154–8164. https://doi.org/10.1029/2019JA026910

Christensen, A. B., Paxton, L. J., Avery, S., Craven, J., Crowley, G., Humm, D. C., et al. (2003). Initial observations with the global ultraviolet imager (GUVI) in the NASA TIMED satellite mission (2003). *Journal of Geophysical Research*, *108*(A12), 1451. https://doi.org/10.1029/2003JA009918

Cierpik, K. M., Forbes, J. M., Miyahara, S., Miyoshi, Y., Fahrutdinova, A., Jacobi, C., et al. (2003). Longitude variability of the solar semidiurnal tide in the lower thermosphere through assimilation of ground- and space-based wind measurements. *Journal of Geophysical Research*, *108*(A5), 1202. https://doi.org/10.1029/2002JA009349

Codrescu, M. V., Codrescu, S. M., & Fedrizzi, M. (2022). Storm time neutral density assimilation in the thermosphere ionosphere with TIDA. *Journal of Space Weather and Space Climate*, *12*, 16. https://doi.org/10.1051/swsc/2022011

Codrescu, M. V., Fuller-Rowell, T. J., & Minter, C. F. (2004). An ensemble-type Kalman filter for neutral thermospheric composition during geomagnetic storms. *Space Weather*, *2*(11), S11002. https://doi.org/10.1029/2004SW000088

Davis, C. J., Wild, M. N., Lockwood, M., & Tulunay, Y. K. (1997). Ionospheric and geomagnetic responses to changes in IMF B_z: A superposed epoch study. *Annales Geophysicae*, *15*(2), 217–230. https://doi.org/10.1007/s005850050435

Doornbos, E., Van Den Ijssel, J., Luhr, H., Forster, M., & Koppenwallner, G. (2010). Neutral density and crosswind determination from arbitrarily oriented multiaxis accelerometers on satellites. *Journal of Spacecraft and Rockets*, *47*(4), 580–589. https://doi.org/10.2514/1.48114

Emmert, J. T., Meier, R. R., Picone, J. M., Lean, J. L., & Christensen, A. B. (2006). Thermospheric density 2002–2004: TIMED/GUVI dayside limb observations and satellite drag. *Journal of Geophysical Research*, *111*(A10), A10S16. https://doi.org/10.1029/2005JA011495

Fok, M.-C., Moore, T. E., Slinker, S. P., Fedder, J. A., Delcourt, D. C., Nosé, M., & Chen, S.-H. (2011). Modeling the superstorm in November 2003. *Journal of Geophysical Research*, *116*(A1), A00J17. https://doi.org/10.1029/2010JA015720

Foster, J. C., Holt, J. M., Musgrove, R., & Evans, D. (1986). Ionospheric convection associated with discrete levels of particle precipitation. *Geophysical Research Letters*, *13*(7), 656–659. https://doi.org/10.1029/GL013i007p00656

Foster, J. C., Coster, A. J., Erickson, P. J., Holt, J. M., Lind, F. D., Rideout, W., et al. (2005). Multiradar observations of the polar tongue of ionization. *Journal of Geophysical Research*, *110*(A9), A09S31. https://doi.org/10.1029/2004JA010928

Fuller-Rowell, T. J., Matsuo, T., Codrescu, M., & Marcos, F. (1999). Modeling thermospheric neutral density waves and holes in response to high latitude forcing. *Advances in Space Research*, *24*(11), 1447–1458. https://doi.org/10.1016/S0273-1177(99)00705-X

Fuller-Rowell, T. J., & Rees, D. (1980). A three-dimensional time-dependent global model of the thermosphere. *Journal of the Atmospheric Sciences*, *37*(11), 2546–2567. https://doi.org/10.1175/1520-0469(1980)037<2545:atdtdg>2.0.co;2

Fuller-Rowell, T. J., Rees, D., Quegan, S., Moffett, R. J., Codrescu, M. V., & Millward, G. H. (1996). A coupled thermosphere ionosphere model (CTIM). STEP Report. In R. W. Schunk (Ed.), *Handbook of ionospheric models* (pp. 217–238). Elsevier.

Gardner, L. C., Schunk, R. W., Scherliess, L., Eccles, V., Basu, S., & Valladeres, C. (2018). Modeling the midlatitude ionosphere storm-enhanced density distribution with a data assimilation model. *Space Weather*, *16*(10), 1539–1548. https://doi.org/10.1029/2018SW001882

Han, J., & Pan, H.-L. (2011). Revision of convection and vertical diffusion schemes in the NCEP Global Forecast System. *Weather and Forecasting*, *26*(4), 520–533. https://doi.org/10.1175/WAF-D-10-05038.1

Hinteregger, H. E., Fukui, K., & Gilson, B. R. (1981). Observational, reference, and model data on solar EUV from measurements on AE-E. *Geophysical Research Letters*, *8*(11), 1147–1150. https://doi.org/10.1029/GL008i011p01147

Juang, H.-M. H. (2011). A multiconserving discretization with enthalpy as a thermodynamic prognostic variable in generalized hybrid vertical coordinates for the NCEP Global Forecast System. *Monthly Weather Review*, *139*(5), 1583–1607. https://doi.org/10.1175/2010MWR3295.1

Juang, H.-M. H. (2014). A discretization of deep-atmospheric nonhydrostatic dynamics on generalized hybrid vertical coordinates for NCEP global spectral model. *NCEP Office Note*, *477*, 39. Retrieved from http://www.lib.ncep.noaa.gov/ncepofficenotes/files/on477.pdf

Liu, H., & Lühr, H. (2005). Strong disturbance of the upper thermospheric density due to magnetic storms: CHAMP observations. *Journal of Geophysical Research*, *110*(A9), A09S29. https://doi.org/10.1029/2004JA010908

Liu, H., Lühr, H., Henize, V., & Ko¨hler, W. (2005). Global distribution of the thermospheric total mass density derived from CHAMP. *Journal of Geophysical Research*, *110*(A4), A04301. https://doi.org/10.1029/2004JA010741

Lomidze, L., & Scherliess, L. (2015). Estimation of thermospheric zonal and meridional winds using a Kalman filter technique. *Space Weather*, *13*(11), 747–760. https://doi.org/10.1002/2015SW001250

Matsuo, T., Lee, I.-T., & Anderson, J. L. (2013). Thermospheric mass density specification using an ensemble Kalman filter. *Journal of Geophysical Research: Space Physics*, *118*(3), 1339–1350. https://doi.org/10.1002/jgra.50162

Mehta, P. M., Linares, R., & Sutton, E. K. (2019). Data-driven inference of thermosphere composition during solar minimum conditions. *Space Weather*, *17*(9), 1364–1379. https://doi.org/10.1029/2019SW002264

Mehta, P. M., Walker, A. C., Sutton, E. K., & Godinez, H. C. (2017). New density estimates derived using accelerometers on board the CHAMP and GRACE satellites. *Space Weather*, *15*(4), 558–576. https://doi.org/10.1002/2016SW001562

Meier, R., Crowley, G., Strickland, D. J., Christensen, A. B., Paxton, L. J., Morrison, D., & Hackert, C. L. (2005). First look at the 20 November 2003 superstorm with TIMED/GUVI: Comparisons with a thermospheric global circulation model. *Journal of Geophysical Research*, *110*(A9), A09S41. https://doi.org/10.1029/2004JA010990

Mlynczak, M. G., Knipp, D. J., Hunt, L. A., Gaebler, J., Matsuo, T., Kilcommons, L. M., & Young, C. L. (2018). Space-based sentinels for measurement of infrared cooling in the thermosphere for space weather nowcasting and forecasting. *Space Weather*, *16*(4), 363–375. https://doi.org/10.1002/2017SW001757

NCEP. (2015). *NCEP GFS 0.25 degree global forecast grids historical archive*. National Center for Atmospheric Research, Computational and Information Systems Laboratory. https://doi.org/10.5065/D65D8PWK

Paxton, L. J., Christensen, A. B., Humm, D. C., Ogorzalek, B. S., Pardoe, C. T., Morrison, D., et al. (1999). Global ultraviolet imager (GUVI): Measuring composition and energy inputs for the NASA thermosphere ionosphere mesosphere energetics and dynamics (TIMED) mission. *Proceedings of SPIE*, *3756*, 265–276. https://doi.org/10.1117/12.366380

Paxton, L. J., Strickland, D. J., Weiss, M., & Meng, C.-I. (1998). Interactive data analysis and display of far ultraviolet data. *COSPAR Adv. Space Res.*, *22*(11), 1577–1582. https://doi.org/10.1016/S0273-1177(99)00116-7

Richards, P. G., Fennelly, J. A., & Torr, D. G. (1994). Euvac: A solar EUV flux model for aeronomic calculations. *Journal of Geophysical Research*, *99*(A5), 8981–8992. https://doi.org/10.1029/94JA00518

Ruan, H., Lei, J., Dou, X., Liu, S., & Aa, E. (2018). An exospheric temperature model based on CHAMP observations and TIEGCM simulations. *Space Weather*, *16*(2), 147–156. https://doi.org/10.1002/2017SW001759

Schlegel, K., Luhr, H., St.-Maurice, J.-P., Crowley, G., & Hackert, C. (2005). Thermospheric density structures over the polar regions observed with CHAMP. *Annales Geophysicae*, *23*(5), 1659–1672. https://doi.org/10.5194/angeo-23-1659-2005

Schoendorf, J., Crowley, G., & Roble, R. G. (1996). Neutral density cells in the high latitude thermosphere – 2. Mechanisms. *Journal of Atmospheric and Terrestrial Physics*, *58*(15), 1769–1781. https://doi.org/10.1016/0021-9169(95)00166-2

Schoendorf, J., Crowley, G., Roble, R. G., & Marcos, F. (1996). Neutral density cells in the high latitude thermosphere – 1. Solar maximum cell morphology and data analysis. *Journal of Atmospheric and Terrestrial Physics*, *58*(15), 1751–1768. https://doi.org/10.1016/0021-9169(95)00165-4

Siemes, C., Borries, C., Bruinsma, S., Fernandez-Gomez, I., Hładczuk, N., van den IJssel, J., et al. (2023). New thermosphere neutral mass density and crosswind datasets from CHAMP, GRACE, and GRACE-FO. *Journal of Space Weather and Space Climate*, *13*, 16. https://doi.org/10.1051/swsc/2023014

Sutton, E. K. (2009). Normalized force coefficients for satellites with elongated shapes. *Journal of Spacecraft and Rockets*, *46*(1), 112–116. https://doi.org/10.2514/1.40940

Sutton, E. K. (2011a). *Accelerometer-derived atmospheric densities from the CHAMP and GRACE accelerometers: Version 2.3*. DTIC# ADA537198. AFRL Technical Memo.

Sutton, E. K. (2011b). Accelerometer-derived atmospheric density from the CHAMP and GRACE satellites (version 2.3) [Dataset]. *Zenodo*. https://doi.org/10.5281/zenodo.13287613

Sutton, E. K. (2018). A new method of physics-based data assimilation for the quiet and disturbed thermosphere. *Space Weather*, *16*(6), 736–753. https://doi.org/10.1002/2017SW001785

Sutton, E. K., Forbes, J. M., & Nerem, R. S. (2005). Global thermospheric neutral density and wind response to the severe 2003 geomagnetic storms from CHAMP accelerometer data. *Journal of Geophysical Research*, *110*(A9), A09S40. https://doi.org/10.1029/2004JA010985

Sutton, E. K., Nerem, R. S., & Forbes, J. M. (2007). Density and winds in the thermosphere deduced from accelerometer data. *Journal of Spacecraft and Rockets*, *44*(6), 1210–1219. https://doi.org/10.2514/1.28641

TIMED/GUVI. (2014). Neutral density profiles (NDP) products (version 13) [Dataset]. Retrieved from https://guvitimed.jhuapl.edu/data_fetch_l2b_ndp_idlsave

Weimer, D. R. (2005). Improved ionospheric electrodynamic models and application to calculating Joule heating rates. *Journal of Geophysical Research*, *110*(A5), A05306–A05321. https://doi.org/10.1029/2004JA010884

Weimer, D. R., Mehta, P. M., Licata, R. J., & Tobiska, W. K. (2023). Global variations in the time delays between polar ionospheric heating and the neutral density response. *Space Weather*, *21*(4), e2022SW003410. https://doi.org/10.1029/2022SW003410

Weimer, D. R., Mehta, P. M., Tobiska, W. K., Doornbos, E., Mlynczak, M. G., Drob, D. P., & Emmert, J. T. (2020). Improving neutral density predictions using exospheric temperatures calculated on a geodesic, polyhedral grid. *Space Weather*, *18*(1), e2019SW002355. https://doi.org/10.1029/2019SW002355

Yang, F., Mitchell, K., Hou, Y., Dai, Y., Zeng, X., Wang, Z., & Liang, X. (2008). Dependence of land surface albedo on solar zenith angle: Observations and model parameterizations. *Journal of Applied Meteorology and Climatology*, *47*(11), 2963–2982. https://doi.org/10.1175/2008JAMC1843.1

Yang, F., Pan, H., Krueger, S. K., Moorthi, S., & Lord, S. J. (2006). Evaluation of the NCEP global forecast system at the ARM SGP site. *Monthly Weather Review*, *134*(12), 3668–3690. https://doi.org/10.1175/MWR3264.1